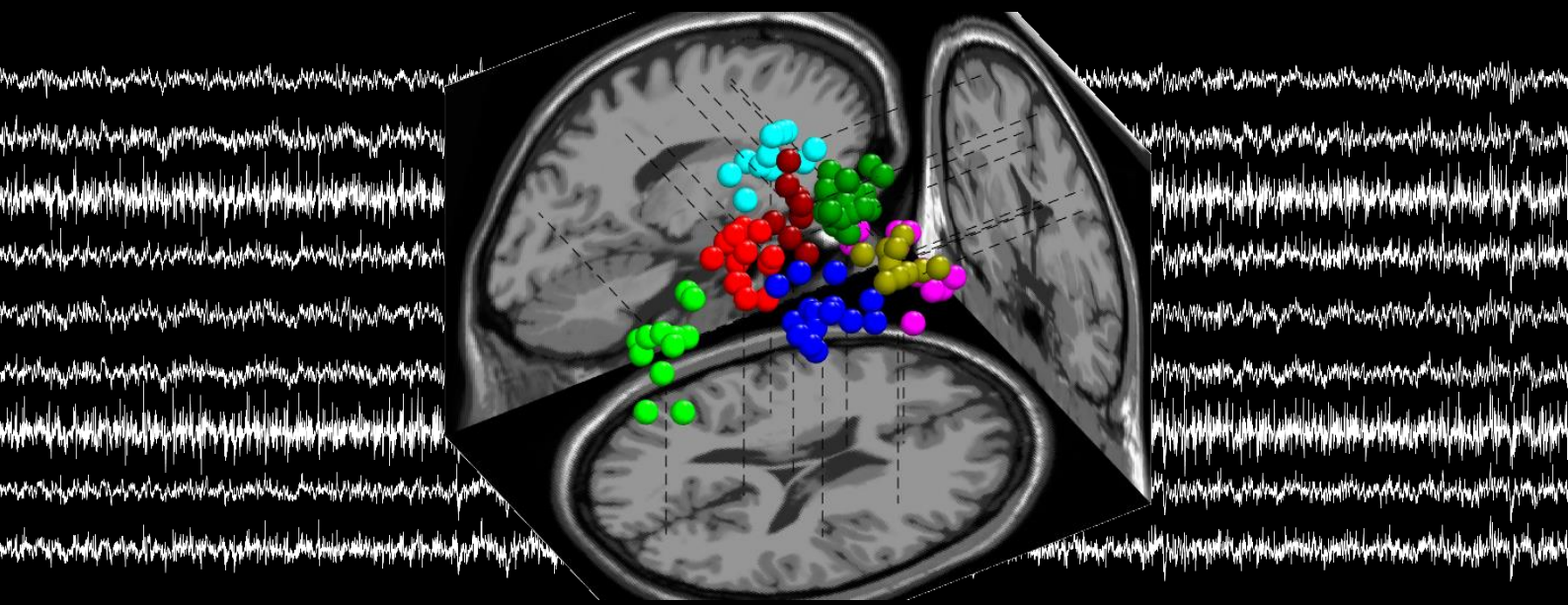


# EEG correlates in the modulation of joint stiffness during posture control of the upper limb

Kirsten Nijmeijer





# EEG correlates in the modulation of joint stiffness during posture control of the upper limb

by

Kirsten Nijmeijer

in partial fulfilment of the requirements for the degree of

**Master of Science**  
in Biomedical Engineering

at the Delft University of Technology  
to be defended publicly on 17 December 2020 at 12.00

**Student number: 4617924**

## **Thesis committee**

Dr. ir. A.C. Schouten (Chair)

TU Delft, Biomechanical Engineering

Dr. ir. M.L. van de Ruit

TU Delft, Biomechanical Engineering

Dr. ing. L. Marchal-Crespo

TU Delft, Cognitive Robotics

Dr. J.J. van den Dobbelaars

TU Delft, Biomechanical Engineering

*This thesis is confidential and cannot be made public until December 17th, 2022*

An electronic version of this thesis is available at <http://repository.tudelft.nl/>.

[This page intentionally left blank]

## Contents

<b>Introduction</b>	<b>1</b>
<b>Methods</b>	<b>2</b>
Participants .....	2
Experimental procedure .....	3
Disturbance signals .....	4
Data acquisition .....	4
Joint stiffness .....	5
EEG analysis .....	5
Statistical analyses .....	7
<b>Results</b>	<b>7</b>
Joint stiffness .....	7
EEG results .....	8
<b>Discussion</b>	<b>11</b>
Limitations .....	13
Concluding remarks .....	13
<b>Acknowledgements</b>	<b>13</b>
<b>References</b>	<b>13</b>
<b>Appendix A: Supplementary Figures and Tables</b>	<b>16</b>
<b>Appendix B: Participant information letter</b>	<b>20</b>

[This page intentionally left blank]

# EEG correlates in the modulation of joint stiffness during posture control of the upper limb

Kirsten Nijmeijer

*Department of Biomechanical Engineering, Delft University of Technology, Delft, The Netherlands*

## Abstract

The ability to control and adapt joint stiffness is essential in human motor control. Both control loops on the spinal as well as cortical level are likely to play a role in this regulation. However, the cortical mechanisms involved with the online adaptive control of joint stiffness remain largely unresolved. This study aimed at identifying cortical areas associated with the process of joint stiffness modulation using electroencephalography (EEG). EEG was recorded in twelve healthy right-handed individuals performing an active posture control task while receiving continuous random force perturbations applied using a robotic manipulator. To provoke a change in the neuromuscular control strategy, i.e. adaptation of joint stiffness, external viscous loads were applied or removed between tasks or instantaneously within tasks. Linear time-invariant system identification techniques were used to estimate joint stiffness between tasks. Cortical oscillatory dynamics were analysed for eight clusters of independent components, which were found using independent component analysis (ICA) and a subsequent dipole source localization method. Power spectral analysis of the time-invariant trials revealed significant enhancement of theta and beta oscillations in the left sensorimotor cortex (S1/M1) and suppression of delta rhythms in the supplementary motor area (SMA) when external damping was present. Analysis of event-related spectral perturbations (ERSPs) in the time-variant trials revealed delta and theta band enhancement in the SMA and sensorimotor cortex following immediately after external damping removal, as well as broadband enhancement in the prefrontal cortex (anterior cingulate cortex (ACC)). Moreover, we found more pronounced modulations in cortical activity with an unexpected decrease in external damping as compared to an increase in viscous loads. These results suggest that multiple cortical areas are likely to be involved in modulating joint stiffness when stability is at risk being the sensorimotor cortex, SMA and prefrontal cortex, whereas adaptive processes in response to increased stability margins might be regulated on a subcortical level.

Keywords: Electroencephalography (EEG), Joint stiffness modulation, Independent Component analysis (ICA), Event-related spectral perturbations (ERSP)

---

## Introduction

The ability to generate goal-directed movements under a variety of environmental conditions relies on feed-forward and complex feedback processes, which are mediated both on a cortical as well as spinal level. (Scott, 2012, 2016) An important concept in studies directed at human motor control is the definition of mechanical admittance describing the mechanical behavior of joints or limbs. Mechanical admittance relates the (angular) displacement of a joint and the forces acting about it. (Kearney & Hunter, 1990; Mizrahi, 2015) It is an important determinant in task performance for both reaching movements as well as in postural control through resisting the effects of external perturbations. Being able to control

and tune the mechanical admittance of joints is therefore essential in human motor control.

From studies in patients with neurological damage, including Parkinson's disease (R. G. Lee & Tatton, 1975; Mazzoni et al., 2012), cerebral palsy (De Gooijer-Van De Groep et al., 2013) and stroke patients (Meskers et al., 2009), we know that neural commands originating from the brain are likely to play an important role in the control of joint admittance, since these patients have presented with an impaired ability to regulate their joint dynamics as compared to healthy individuals. The cortical mechanisms involved in the adaptation of mechanical admittance, or more specifically joint stiffness, are however still poorly understood. More insights into the key players in joint stiffness regulation is

---

required to improve our understanding of how impaired movement control is affected by a distorted ability to control and tune joint stiffness. Better understanding of this relationship could aid in the diagnosis of motor problems in neurological patients and more personalized rehabilitation plans, e.g. aimed at re-learning adaptation of joint stiffness.

Currently, there are limited studies available that have focused at directly relating cortical control mechanisms and joint stiffness modulation in the upper extremity. However, joint stiffness is composed of two distinct components: an intrinsic stiffness, originating from visco-elastic properties of the joint, muscles and surrounding passive tissue and a reflexive contribution, generated by modifiable stretch reflex muscle responses. (Ludvig & Kearney, 2007) Therefore, studies on the cortical involvement in the regulation of feedback responses could provide potential candidates important in the regulation of joint stiffness.

A number of studies have investigated the role of the primary motor cortex (M1) in the generation and regulation of stretch responses. Whereas a functional link between M1 and the stretch response was already established in early studies by measuring cortical potentials in response to mechanical perturbations preceding the stretch response either invasively in monkeys (Cheney & Fetz, 1984; Evarts & Tanji, 1976; Fromm & Evarts, 1977) or non-invasively in humans (Abbruzzese et al., 1985; MacKinnon et al., 2000), the use of techniques like transcranial magnetic stimulation (TMS) provide even stronger evidence for a critical role of M1 in the regulation of joint stiffness. (Kimura et al., 2006; Shemmell et al., 2009) In both studies, they found that applying TMS over M1, which induces a period of cortical inhibition, resulted in loss of reflex gain adaptation. A similar effect was seen by applying TMS over the supplementary motor area (SMA) suggesting that the SMA might also be important in the process of setting feedback gains thereby influencing joint stiffness. (Spieser et al., 2013) In a study done by Omrani et al., they mapped the cortical activity over time relative to a mechanical disturbance in monkeys performing different tasks. They found increased activity in the posterior parietal cortex (PPC) as well as in the premotor cortex (PMC) already after ~25 ms post-perturbation during postural tasks. (Omrani et al., 2016) Whereas no causal implications can be derived from this observation, it does open a window for the PMC and PPC to be involved in regulation of the feedback responses based on the timing of the measured activity. However, none of the studies presented here investigated the adaptation process over time and the cortical processes responsible for online control of joint stiffness remain largely unexplored.

One way to gain more insights into brain areas contributing to joint stiffness modulation is through measurement of brain activity using electroencephalography (EEG) while evoking an adaptive mechanical response. Previous studies have shown that joint stiffness is modulated in response to an alteration in the environmental dynamics. (De Vlugt et al., 2002; Perreault et al., 2008; Schouten et al., 2008) Therefore, we used an experimental

paradigm in which participants had to maintain the position of their right arm under variable environmental conditions while being perturbed continuously. During these tasks, EEG was measured. EEG records the electrical activity of the brain at the scalp-level with high temporal precision, but the recorded signal at each electrode is a mixture of source signals through volume conduction. (Makeig et al., 1996) To study the contribution of individual cortical areas, blind source separation and source localization techniques are required. Application of an independent component analysis (ICA) followed by a model fit of a single equivalent current dipole is often used to separate the EEG data in physiologically and spatially distinct sources. (Delorme et al., 2012; Makeig et al., 2004) Time-frequency analysis can then be used to investigate changes in the spectral characteristics of cortical activity on a source level elicited by an unexpected change in the environmental dynamics. Analysis of cortical activity in the frequency domain is preferred over studying the event-related potentials (ERPs), since brain dynamics are of oscillatory nature and ERPs cannot fully capture changes in oscillatory behavior. (Makeig, 1993) Additionally, different rhythms can be studied and therefore be related to adaptive motor control. Previous studies have associated low-frequency cortical rhythms (<12 Hz; theta and alpha rhythms) with cognitive processes, memory and perception (Cavanagh & Frank, 2014; Klimesch, 1999), whereas high-frequency cortical rhythms (>12 Hz; beta rhythms) have been associated with maintaining a sensorimotor state. (Engel & Fries, 2010)

In this study we aimed to identify cortical areas involved in the online adaptation of joint stiffness. Combining an experiment that provokes adaptation of joint stiffness using continuous disturbances with EEG measurement allows for investigating the role of cortical areas in stiffness adaptation over time, which is a novel approach in the area of adaptive motor control studies. We expect to find a role for the cortical areas that have been associated with regulation of feedback responses before, among which the primary motor cortex (M1), the supplementary motor area (SMA), the posterior parietal cortex (PPC) and the premotor cortex (PMC). However, since there are limited studies that have focused on identifying the role of brain areas other than M1 in relation to modulation of joint stiffness over time, this study is mainly of exploratory nature.

## Methods

### Participants

Twelve healthy volunteers were recruited for participation in this study (age:  $25 \pm 2$  years; eight female), which were all right-handed. All participants were instructed to withhold from any caffeinated drinks on the day of the experiment and gave written informed consent prior to the experiment. The study was performed in the Laboratory for NeuroMuscular Control within the department of Biomechanical Engineering of the Delft University of Technology

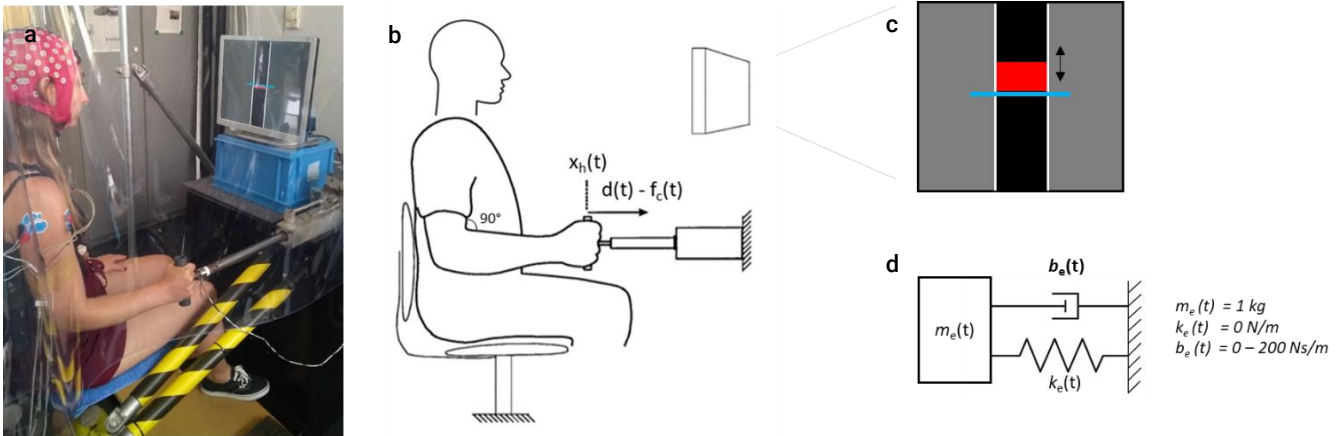


**Figure 1 | Experimental set-up.** The participant is seated in front of the 1-DoF robotic manipulator and holds the handle connected to the moving piston with their right hand. **(a)** The forearm is aligned with the piston and a 90-degree angle with the upper arm is ensured marking the reference position. The handle position ( $x_h(t)$ ) is controlled by the disturbance force ( $d(t)$ ) and the force applied by the participant ( $f_c(t)$ ). (Adapted from Van Der Helm et al., 2002) **(b)** Visual feedback is displayed on the monitor in front of the participant and shows the static reference (target) position (blue line) and the deviation thereof (red area). **(c)** The virtual environment can be represented by a mass-spring damper system with constant values for the mass ( $m_e$ ) and stiffness ( $k_e$ ), whereas damping ( $b_e(t)$ ) was set to either 0 or 200 Ns/m and changed instantaneously within time-variant trials. **(d)**

and was approved by the Human Research Ethics Committee TU Delft.

## Experimental procedure

### Experimental set-up

Force perturbations were applied using a linear hydraulic robotic manipulator with one degree-of-freedom. (Van Der Helm et al., 2002) Participants were seated in front of the robotic manipulator and firmly held on to the handle with their right hand. Their forearm was aligned with the moving piston and made a 90-degree angle with the upper arm in the reference position. (see Figure 1a, b) Movement of the handle was constrained to longitudinal movement only and therefore the handle position directly translates to the position of the gleno-humeral joint. Forward and backward movements of the handle result in flexion and extension at the shoulder level, respectively.

The position of the handle ( $x_h(t)$ ) is controlled by the manipulator based on the disturbance force ( $d(t)$ ), the hand reaction force ( $f_c(t)$ ) and the dynamics of the simulated virtual environment. (see Figure 1b, d) The manipulator acts like a mass-spring-damper system of which the parameters can be varied. By adjusting the parameters, the interaction of the human with different environmental dynamics can be studied thereby obtaining insight into human neuromuscular control strategies. (Krutky et al., 2010; Perreault et al., 2008; Schouten et al., 2008) In this study, we aimed to evoke joint stiffness adaptation by adjusting the external damping values, which has been shown before to result in adjusted reflex gains in the shoulder. (Schouten et al., 2008) Therefore, the damping value ( $b_e(t)$ ) was set to either 0 or 200 Ns/m and varied over time within time-variant trials (see 'Experimental protocol'). The virtual mass ( $m_e$ ) was set to a

constant value of 1.6 kg and no virtual spring was used in this study ( $k_e = 0$  N/m). (see Figure 1d)

### Task

Participants performed a position task with their right arm while receiving continuous random force perturbations applied by the robotic manipulator. The participants were verbally instructed to minimize the displacement. Visual feedback was provided by projecting the reference and the actual handle position on a screen thereby aiding in task performance and preventing drift from the reference position. (see Figure 1c)

### Experimental protocol

After ensuring the participant was seated in the correct position by setting the reference position of the handle, a gain factor for the force disturbances was determined for both the zero ( $b_e = 0$  Ns/m) and the high ( $b_e = 200$  Ns/m) external damping condition. By applying a different gain factor for both conditions, similar sized small position deviations can be obtained for both environmental settings. This ensures a comparable situation in terms of muscle stretch and allows for the use of linear model approximations. The gain factor was set to obtain a root-mean-square value (RMS) of approximately 3 mm for the handle position. The trials used for this scaling also served as training trials to familiarize the participants with the task and were performed at least thrice for each condition. The training trials were not included in the analysis.

The main experimental session consisted of a total of 96 trials, which lasted between 20-40 seconds depending on the number of damping transitions contained in the trial and were divided into four blocks of 24 trials. To prevent fatigue and to preserve participant's concentration short obligatory breaks of 5-15 minutes were implemented between these blocks.

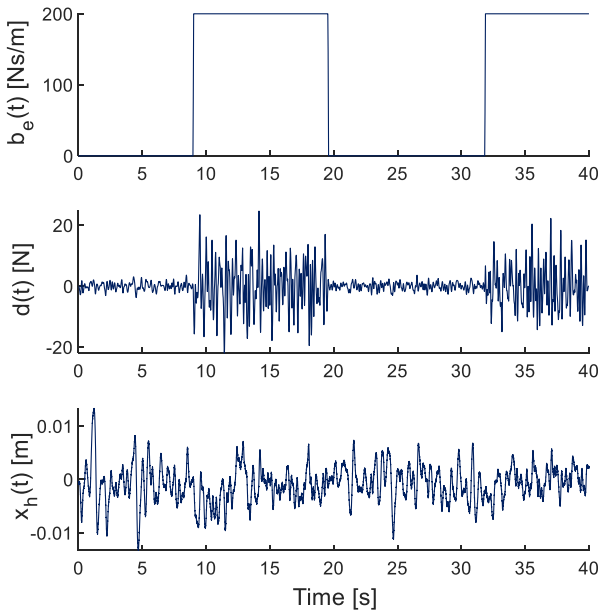


**Figure 2 | Example of signals for a time-variant task with three events.** The top panel contains an example of the damping profile  $b_e(t)$  for a time-variant condition starting with zero damping and having three damping transitions. Damping is changed in 100 ms between 0 and 200 Ns/m. The middle panel depicts the disturbance force  $d(t)$  with the scaling factors applied. The measured handle position  $x_h(t)$  is shown in the bottom panel illustrating similar sized position deviations when damping is either 0 or 200 Ns/m.

Two types of trials were included being time-invariant trials in which the external damping value remained constant (0 or 200 Ns/m; 25% of the trials) and time-variant trials. During time-variant trials the external damping value was increased or decreased from 0 to 200 Ns/m (or v.v.) in 100 milliseconds at least twice and maximally four times per trial. These switches (i.e. damping transitions) were implemented at random time intervals to minimize participant's ability to predict when a damping transition was to be expected. (see Supplementary Figure 1) The time in between switches was constrained at 8 seconds minimum to ensure participants fully adapted and reached a steady-state before being presented with another external damping change. In figure 2, an example of a damping profile for a time-variant task is shown together with the scaled applied disturbance force and the resulting handle position. In total, 216 damping transitions were contained in the time-variant trials with an equal distribution between damping increases and decreases. Time-variant and time-invariant trials were presented in a pseudo-randomized order.

To minimize the effect of surrounding noise in the EEG measurement, participants were asked to wear earplugs.

## Disturbance signals

To stimulate the somatosensory nervous system and to challenge task execution, continuous random force perturbations were applied during the position task. The disturbance forces were generated offline and a different disturbance force was applied each trial. The type of signal used for perturbation was a filtered white Gaussian noise (bandwidth between 0.5 and 7 Hz; low-pass third-order and high-pass fourth-order Butterworth zero-phase filter). Perturbation signals were selected from 10000 filtered white Gaussian noise realizations to ensure signals with outlier amplitudes were removed and to obtain signals with the most uniform power distribution and the lowest possible correlation.

A first selection was performed based on the peak-to-rms value (or crest factor) using a threshold of  $<3.5$  thereby removing 85-90% of the signals. To ensure the disturbance signals contained an equal amount of power for all frequencies within the bandwidth, signals were selected based on their mean power within the frequency bandwidth and the distribution of power over the frequencies. Power spectra were computed using Welch's method and z-scores<sup>1</sup> for the mean and SD of the power spectra were used to remove 13-15% of the remaining signals. Realizations having a z-score  $< -1.5$  for the mean power or a z-score  $> 1.5$  for the SD of the power distribution were removed. (see Supplementary Figure 2) Subsequently, the realizations with a correlation coefficient less than 0.1 were obtained and 96 signals were randomly selected from the remaining signals. This selection process was repeated for every participant resulting in different sets of disturbance signals with similar characteristics for each participant.

## Data acquisition

High-density EEG data was acquired using a cap with 128 Ag/AgCl electrodes (Waveguard, ANT Neuro, The Netherlands) arranged according to the 10-5 system. (Oostenveld & Praamstra, 2001) The mastoid electrodes integrated in the cap were not used. A separate electrode (Blue Sensor N, Ambu, Ballerup, Denmark) was connected to the right mastoid and served as the participant ground. EMG signals from four shoulder muscles (m. deltoid anterior; m. deltoid posterior; m. pectoralis major; m. latissimus dorsi) were recorded using pairs of unipolar electrodes (Bleu Sensor N, Ambu) placed on the skin. EEG and EMG signals were recorded at 2048 Hz using a Refa amplifier (TMSi, Oldenzaal, The Netherlands) without any filters (only anti-alias filter). EMG signals were however not used in the analysis of this study and were recorded to complement future studies on this topic. Additionally, the handle position ( $x_h(t)$ ), disturbance force ( $d(t)$ ) and measured contact force ( $f_c(t)$ ) were recorded at 2048 Hz from the robotic manipulator using optical isolation amplifiers (TMSi, Oldenzaal).

<sup>1</sup> Z-scores indicate the deviation from average expressed in standard deviations:  $Z_i = \frac{x_i - \mu}{\sigma}$

## Joint stiffness

To analyse the change in arm dynamics with varying external damping values, joint stiffness was estimated using linear time-invariant system identification techniques in the frequency domain. Closed-loop identification algorithms were applied, because the handle position depends both on the dynamics of the manipulator as well as on the participant's dynamics. (see Figure 3) Applied disturbance forces  $d(t)$  affect the handle position  $x_h(t)$  dependent on the dynamics of the manipulator and handle position in turn influences the contact force  $f_c(t)$ . Therefore, the handle position and the contact force are dependent variables, while the disturbance force is independent. The frequency response function (FRF) of the arm ( $\hat{H}_{arm}$ ) relating the displacements of the limb to the input force, i.e. the mechanical admittance, was estimated as follows (Schouten et al., 2008; Van Der Helm et al., 2002)

$$\hat{H}_{arm}(f) = \frac{\hat{S}_{dx}(f)}{\hat{S}_{df}(f)} \quad (1)$$

with  $\hat{S}_{dx}$  and  $\hat{S}_{df}$  being estimates of the spectral densities between  $d(t)$  and  $x_h(t)$  or  $f_c(t)$ , respectively. Additionally, a measure of linear dependency between the two signals, the coherence ( $\hat{\gamma}^2$ ) was calculated as follows

$$\hat{\gamma}^2(f) = \frac{|\hat{S}_{dx}(f)|^2}{\hat{S}_{dd}(f)\hat{S}_{xx}(f)} \quad (2)$$

Coherence varies between 0 and 1 and is reduced by external noise sources and non-linearities between the signals. (Schouten et al., 2008; Van Der Helm et al., 2002)

Mechanical admittance and coherence were calculated for the two conditions having a constant external damping value of 0 or 200 Ns/m using the measurements from the time-invariant trials. Only the time-invariant trials were analysed, because analysing the course of the mechanical admittance in time-varying trials requires time-variant identification techniques, which is beyond the scope of this study. The first and last two seconds of each trial were excluded from the analysis leaving 12 trials of 16 s per condition (=192 s in total). The (cross) power spectral densities were estimated using Welch's averaged periods of 5 s with an overlap of 50% and a Hanning window giving a frequency resolution of 0.2 Hz. The FRFs and coherence were estimated up to 10 Hz, since the perturbation signal was low-pass filtered at 7 Hz and therefore contained zero-power in higher frequencies.

Joint stiffness was estimated from the admittance value around 1 Hz, because it is at the low frequencies (below the eigenfrequency) that the FRF is dominated by the effect of stiffness, whereas with increasing frequency muscle viscosity and inertial properties are more dominant. (Van Der Helm et al., 2002) The mechanical admittance was averaged over three frequencies (0.8, 1.0 and 1.2 Hz) having a coherence  $>0.75$  and stiffness was calculated as the inverse of the averaged admittance value for both conditions.

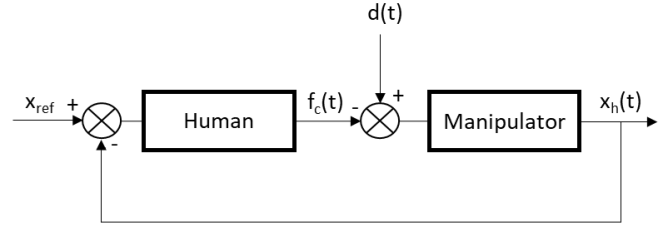


**Figure 3 | Control scheme illustrating the closed-loop configuration between the manipulator and the human during posture control.** The external force perturbation  $d(t)$  and the contact force  $f_c(t)$  produced by the human determine the handle position  $x_h(t)$  dependent on the dynamics of the manipulator. In turn, the human produces a contact force  $f_c(t)$  to maintain the reference position  $x_{ref}$  performing a posture control task. The external disturbance force  $d(t)$ , the contact force  $f_c(t)$  and the handle position  $x_h(t)$  are measured signals.

## EEG analysis

The acquired EEG data was processed using custom scripts in MATLAB (The Mathworks, Inc., Natick, MA, USA) and incorporating functions from the open-source EEGLAB toolbox. (Delorme & Makeig, 2004) A summary of the processing pipeline is given in figure 4. Each processing step will be elaborated on below.

### Pre-processing

The continuous EEG data was resampled to 256 Hz (using a FIR anti-aliasing filter) and filtered between 0.5 and 120 Hz (fourth-order Butterworth zero-phase filter). Additionally, band-stop filters with a bandwidth of 2 Hz (fourth-order Butterworth zero-phase filter) were applied around 50 and 100 Hz to reduce line noise and its harmonic. Bad channels identified by a high impedance during the recording and channels having a SD with a z-score higher than three were removed ( $6 \pm 4$  channels). The remaining channels were re-referenced to the common average. The data segments corresponding to the trials were extracted (96 epochs; 40 seconds each) from the pre-processed continuous EEG data and were used for further processing.

### Independent Component analysis

To separate brain activity from other artefactual (e.g. cable movement) and physiological (e.g. eye blinks, muscle activity) sources, an independent component analysis (ICA) was performed. (Jung et al., 2001; Makeig et al., 1996) All data segments were processed with *binica*, a function from the EEGLAB toolbox, which uses the extended Infomax ICA algorithm. (Bell & Sejnowski, 1995; T. W. Lee et al., 1999) The independent component analysis identifies components with maximally independent activity time courses, which therefore most likely represent physiologically or functionally distinct electrocortical processes. (Makeig et al., 2004) The ICA results in a set of spatial filters, together also called the

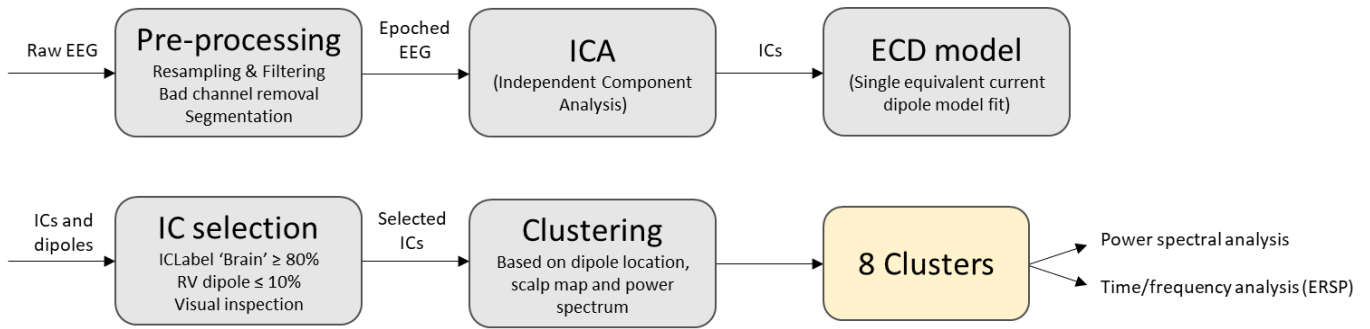


**Figure 4 | Overview of processing pipeline EEG data.** Raw EEG data was processed to obtain a number of clusters containing independent components from more than half of the participants with similar characteristics and a physiologically relevant cortical centroid location. The resulting clusters of independent components were then subject to a power spectral analysis for the time-variant trials and a time/frequency analysis for the time-invariant trials studying the event-related spectral perturbations (ERSPs).

unmixing matrix, which transforms the scalp data into the component activities by matrix multiplication:

$$U = WX \quad (3)$$

where  $W$  is the unmixing matrix,  $X$  contains the measured scalp potentials and  $U$  represents the component activity time courses. Subsequent analysis was performed using component activity rather than electrode signals, since the latter represents a mixture of the underlying physiological relevant sources, whereas the aim of the independent component analysis is to separate these into spatially stationary distinct components.

### Equivalent current dipole model

To estimate where the independent component (IC) activity originates from, a single equivalent current dipole (ECD) was fitted to each IC's scalp projection. This was done using DIPFIT3 routines implemented in EEGLAB, which finds the dipole location within a 3D head model best explaining the dipolar scalp projection using non-linear optimization techniques. (Delorme et al., 2012; Delorme & Makeig, 2004) The 3D head model used was a three-shell boundary element head model together with standard electrode positions from the MNI template, as implemented in the DIPFIT3 toolbox. Using ICA and a subsequent ECD model fit has been argued to be an effective way of performing source localization and has been used before to analyse and localize changes in cortical activity evoked by stimuli or between different conditions. (Chikara & Ko, 2019; Delorme et al., 2012; Makeig et al., 2004; Solis-Escalante et al., 2019)

### Component selection and clustering

To select the components representing brain activity, ICs were classified using ICLabel, an automated classifier which gives probability measures for seven different classes (e.g. 'brain' or 'muscle') per component based on key features like component topography, power spectral density (PSD) measures and the autocorrelation function. (Pion-Tonachini et al., 2019) Furthermore, ICs were selected on the residual variance (RV) from the ECD model fit, which indicates how well the fitted dipole

explains the scalp projection. ICs which were classified as 'Brain' with a probability of  $\geq 80\%$  and had a dipole fitted with a residual variance  $\leq 10\%$  were continued with ( $16 \pm 7$  ICs per participant). Additionally, a visual inspection was performed to eliminate components with physiologically irrelevant locations. (see Supplementary Figures 3 and 4 for an example of scalp maps with their fitted dipoles and the visual selection)

The remaining number of ICs from all participants ( $13 \pm 5$  ICs per participant, see Supplementary Table 1) were subject to a clustering routine to obtain sets of components with quantitatively similar characteristics. Clustering was based on dipole locations ( $x,y,z$ -coordinates), component scalp maps and power spectrum between 2 and 48 Hz. The dimensions of the scalp map and power spectrum measures were reduced through principal component analysis to three and six, respectively. Since the aim of the clustering procedure is to define clusters of components representing the activity of a localized cortical region, dipole locations were weighted twice in the clustering routine. Clustering relied on the k-means algorithm and the number of clusters ( $k=13$ ) was chosen equal to the median of the number of components per participant. The centroid locations (average of IC dipole locations) of the resulting clusters were used to determine the cortical origin of the grouped ICs using Talairach Client. (Lancaster et al., 2000) Only those clusters containing components from more than half of the subjects and having a centroid location in a physiologically relevant cortical location were further analysed. Subsequent analysis was performed on the clusters to generalize the results for a participant-specific individual component to results for a cortical region.

### Power spectral analysis

To analyse the cortical dynamics in both the zero-damping and high-damping condition independent of the adaptation process, the relative change in power of brain oscillations between the time-invariant trials was computed.

For each component, the power spectral density (PSD) was computed using Welch's averaging with segments of 2s having 50% overlap and using a Hanning window. The first and last two

seconds of each trial were excluded to remove settling in effects. The PSDs were averaged over the trials from the same IC and damping condition. The relative change in power between the conditions was calculated by subtracting the log transformed PSD in the zero-damping condition ( $PSD_0$ ) from the log transformed PSD in the high-damping condition ( $PSD_{200}$ ) for each IC individually. For a given IC cluster, the mean relative power change was calculated by averaging the relative power over the component members within the cluster. Differences in the oscillatory behaviour of the brain were determined for the general EEG frequency bands (delta: 1-4 Hz; theta: 4-8 Hz; alpha: 8-12 Hz; beta-I: 12-18 Hz; beta-II: 18-30 Hz) by averaging across the values within these frequency bands.

### Time/frequency analysis: Event-related spectral perturbations

To study the EEG patterns in the frequency domain in response to a changing environment, the event-related spectral perturbation (ERSP) measure was used. (Makeig, 1993) The ERSP computes relative changes in oscillatory dynamics throughout a broad-band frequency range as a function of time.

The pre-processed EEG data from the time-variant trials was segmented between -2 and 5 s relative to the occurrence of an event (damping switch) and split into two datasets based on the direction of the damping change. To identify and reject outlier epochs that could bias the results, PSDs of individual segments were analysed. Segments having an absolute z-score for the power between 2 and 48 Hz higher than 4 were excluded ( $1 \pm 1$  trials per cluster). ERSPs were calculated for each component individually using the *newtimef* function available in EEGLAB. (Delorme & Makeig, 2004) This function allows for the use of Morlet wavelets in the time/frequency decomposition. Using Morlet wavelets has the advantage of being able to adapt the number of cycles used to calculate the time/frequency decomposition dependent on the frequency, which influences the temporal and frequency resolution. Here we used 1.5 cycles at the lowest frequency and a shortening factor of 0.8 to estimate the ERSPs from 1-40 Hz having a satisfactory time/frequency resolution. The ERSP values were calculated relative to the power spectral values of a baseline period, which was set to a 1s time window preceding the event. Mean time/frequency maps for each cluster were calculated as the average across time/frequency maps of individual components within a cluster for the two conditions separately (i.e. damping increase or damping decrease).

### Statistical analyses

The difference in joint stiffness between the constant zero-damping and constant high-damping condition was tested for significance using Wilcoxon's signed rank test. The same test was used for the analysis of the relative power changes in oscillatory brain dynamics between the time-invariant trials by testing whether the modulations found were significantly different from zero for each general frequency band. For the ERSP analysis, permutation-based statistics were used (1000 iterations) to test if

the found ERSP values were significantly different from zero (or baseline). Additionally, a correction for false discovery rate (FDR) was applied. For all tests, a significance threshold of  $\alpha = 0.05$  was used.

## Results

### Joint stiffness

A typical estimate of an FRF, from which joint stiffness was derived, and coherence for one subject are shown in figure 5. In the low-frequency range, the mechanical admittance is decreased in the high-damping condition as compared to the zero-damping environment. Furthermore, the peak around the eigenfrequency of the shoulder ( $\sim 2.5$  Hz) increased with the addition of external damping. The coherence was higher than 0.85 for both conditions between 1 and 6 Hz.

Figure 6 shows the estimated joint stiffness in both time-invariant conditions for each participant separately and averaged on group level. The error bars represent the variability between subjects in one condition depicting the standard error (SE). In 10/12 participants an increase in joint stiffness with added external damping was detected. The average modulation of shoulder stiffness between the tasks was found to be significant on group level ( $n = 12$ ,  $Z = -2.59$ ,  $p < 0.01$ ).

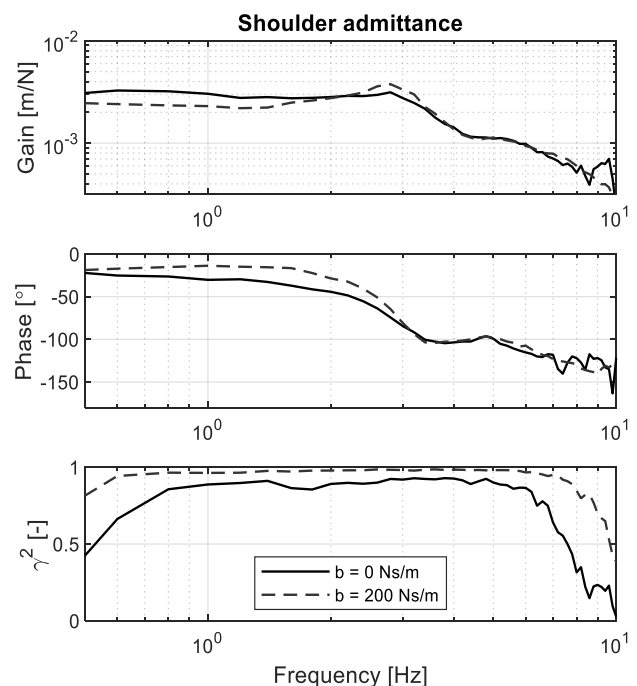


**Figure 5 | FRF and coherence plots.** An estimate of the FRF of the mechanical admittance (gain: top row; phase: middle row) for a typical subject with the corresponding coherence (bottom row) as a function of frequency. The FRF and coherence are plotted for both time-invariant conditions having either constant zero external damping (solid line) or a constant external damping of 200 Ns/m (dotted line).

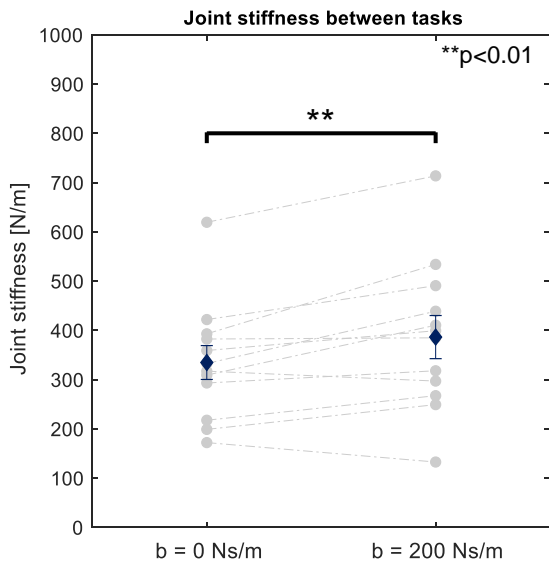


**Figure 6 | Joint stiffness for the time-invariant conditions.** The estimated joint stiffness for the tasks having a constant external damping value of 0 or 200 Ns/m averaged over the participants is depicted by the blue diamonds. The error bars represent the standard error. The joint stiffness for each participant individually is plotted in grey and the two measurements per participant are connected illustrating the trend of increased joint stiffness in the high-damping task as compared to the task without damping. The difference in joint stiffness between the conditions appeared to be significant on group level ( $p < 0.01$ ).

## EEG results

### Clustering

The clustering routine (k-means algorithm;  $k=13$ ) resulted in nine clusters containing ICs from more than half of the participants and having a physiologically relevant location. The total number of clusters selected for further analysis was reduced to eight by merging the two clusters located in the frontal brain region in the left and right hemisphere, since no lateralized effects were expected to occur in this area. Table 1 presents the centroid locations using Talairach coordinates and the associated cortical regions. Figure 7 shows the averaged scalp maps of electrical activity and summarizes the number of unique participants and ICs contained in each cluster. The cluster associated with the SMA contained at least one IC from every participant. The other clusters contained ICs varying from seven to nine participants. (see also Supplementary Table 2) Additionally, the equivalent dipole locations of the individual components are plotted within a standard MRI head model for each cluster in figure 7. Five clusters were found along the sagittal midline of the brain, one cluster on the left hemisphere and two clusters on the right hemisphere.

### Power spectral analysis

The results of the analysis in oscillatory behaviour between the two conditions in time-invariant trials is shown for each cluster in figure 8. The left plot shows the relative power change as a function of

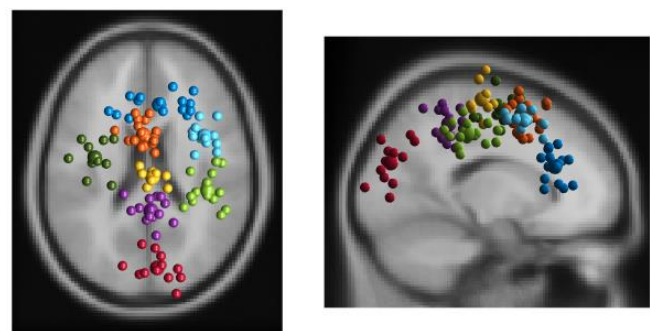
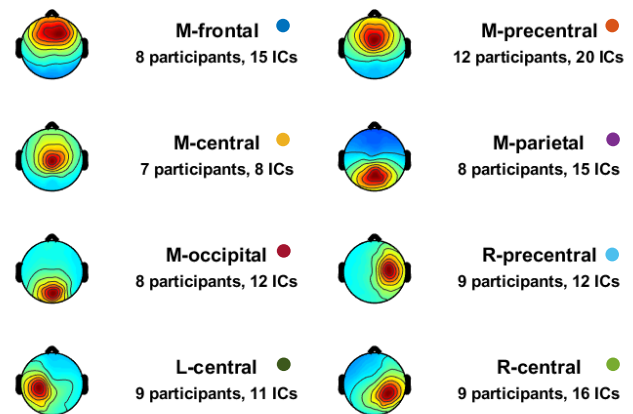


**Figure 7 | Summary of selected clusters.** For each cluster the averaged scalp map of cortical activity is shown. The number of unique participants and ICs contained in each cluster are indicated. The colour dots behind the labels correspond with the associated plotted equivalent dipole locations of each IC within a cluster in the transversal view (bottom left) and sagittal view (bottom right).

**Table 1 | Summary of the estimated cluster locations**

IC cluster label	Centroid location (x,y,z)	Brodmann area	Cortical location
M-frontal	8, 27, 19	BA32	Anterior cingulate cortex
M-precentral	-2, 9, 49	BA6	Supplementary motor area
M-central	4, -18, 62	BA6	Primary motor cortex
M-parietal	2, -40, 48	BA5	Posterior parietal cortex
M-occipital	7, -78, 26	BA18	Visual cortex
R-precentral	38, 8, 48	BA6	Right premotor cortex
L-central	-34, -5, 55	BA6	Left sensorimotor cortex
R-central	40, -27, 41	BA2	Right sensorimotor cortex

frequency, whereas the right plot shows the relative power modulations averaged over the pre-defined EEG frequency bands.

Overall, a limited number of significant power modulations was observed between the two conditions. Most prominent differences were found in the cluster located on the left hemisphere representing the left sensorimotor cortex (L-central). The theta, beta-I and beta-II rhythms in this cortical region were significantly

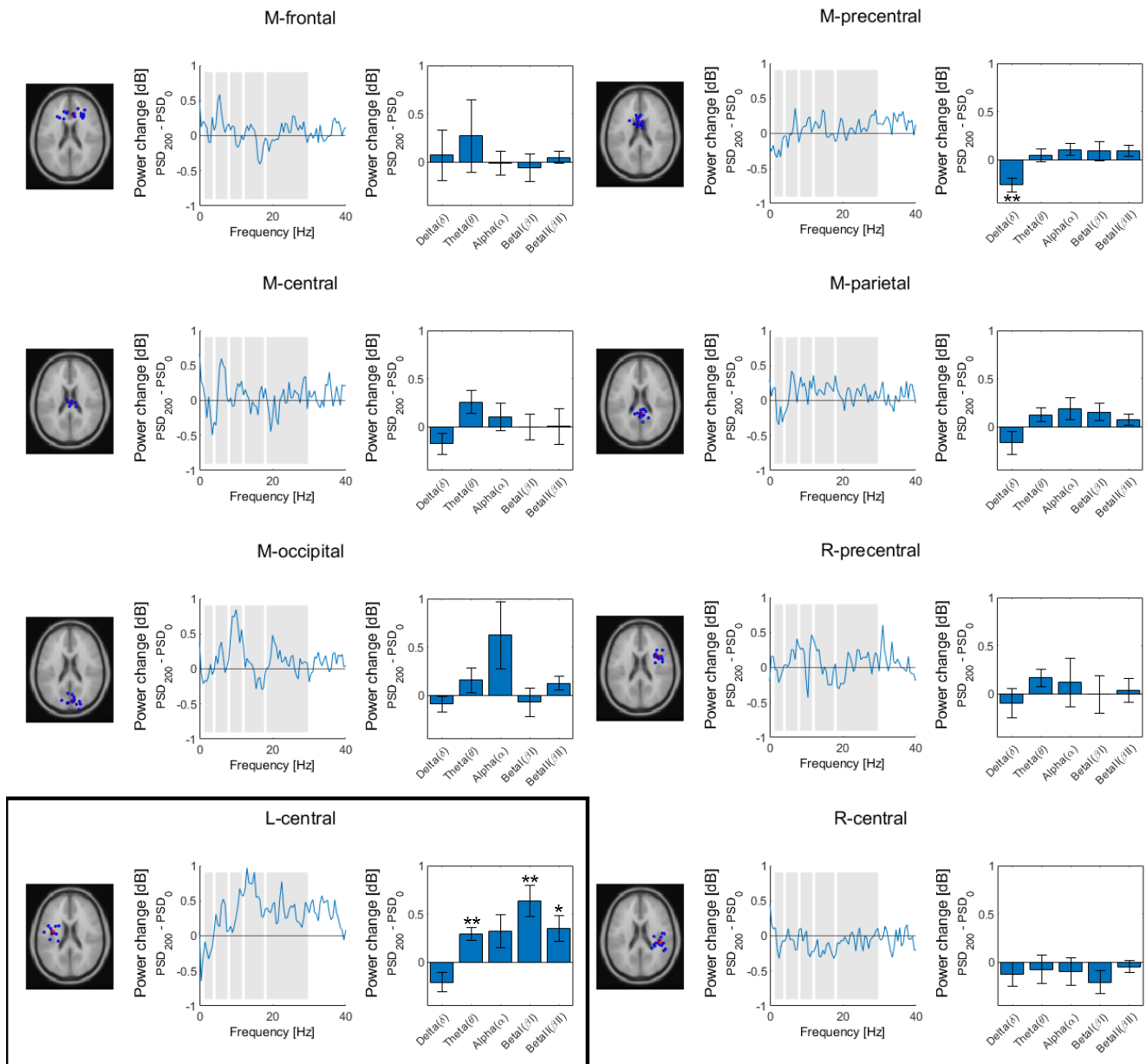


**Figure 8 | Relative power changes in oscillatory brain activity between time-invariant trials across frequencies and frequency bands.** For each cluster the averaged difference between the log transformed power spectral density in the high-damping condition and the zero-damping condition is shown versus frequency in the first plot. The bar graph plots show the power change averaged over the frequencies within general EEG frequency bands (depicted by the grey shaded areas: 1-4 Hz, 4-8 Hz, 8-12 Hz, 12-18 Hz, 18-30 Hz) and the SEs. The graphic on the left shows the dipole locations of the individual components within a cluster (blue spheres) and the centroid location (red sphere). Note that power modulations are most prominent in the L-central cluster (highlighted with the black box). Significant power modulations are indicated with asterisks. (\* $p < 0.05$ , \*\* $p < 0.01$ )

enhanced with external damping added to the environment ( $n = 11$ ; theta:  $Z = 2.67$ ,  $p < 0.01$ ; beta-I:  $Z = 2.67$ ,  $p < 0.01$ ; beta-II:  $Z = 2.22$ ,  $p < 0.05$ ). Furthermore, a significant power decrease in the delta frequency band was observed in the midline precentral (M-precentral) cluster representing the supplementary motor area (SMA) ( $n = 20$ ;  $Z = -2.76$ ,  $p < 0.01$ ).

Whereas the average change in power in the alpha frequency band for the cluster located occipally on the midline (M-occipital) seemed to be considerable, this difference was not found to be

significant. The variance between the power in the individual components was relatively large for this frequency band and similarly for several other clusters as illustrated by the error bars representing the SE.

#### Time/frequency analysis: Event-related spectral perturbations

Average time-frequency maps showing the modulations of oscillatory behaviour in response to a changing environment are shown in figure 9. Two maps are shown for each cluster, depicting

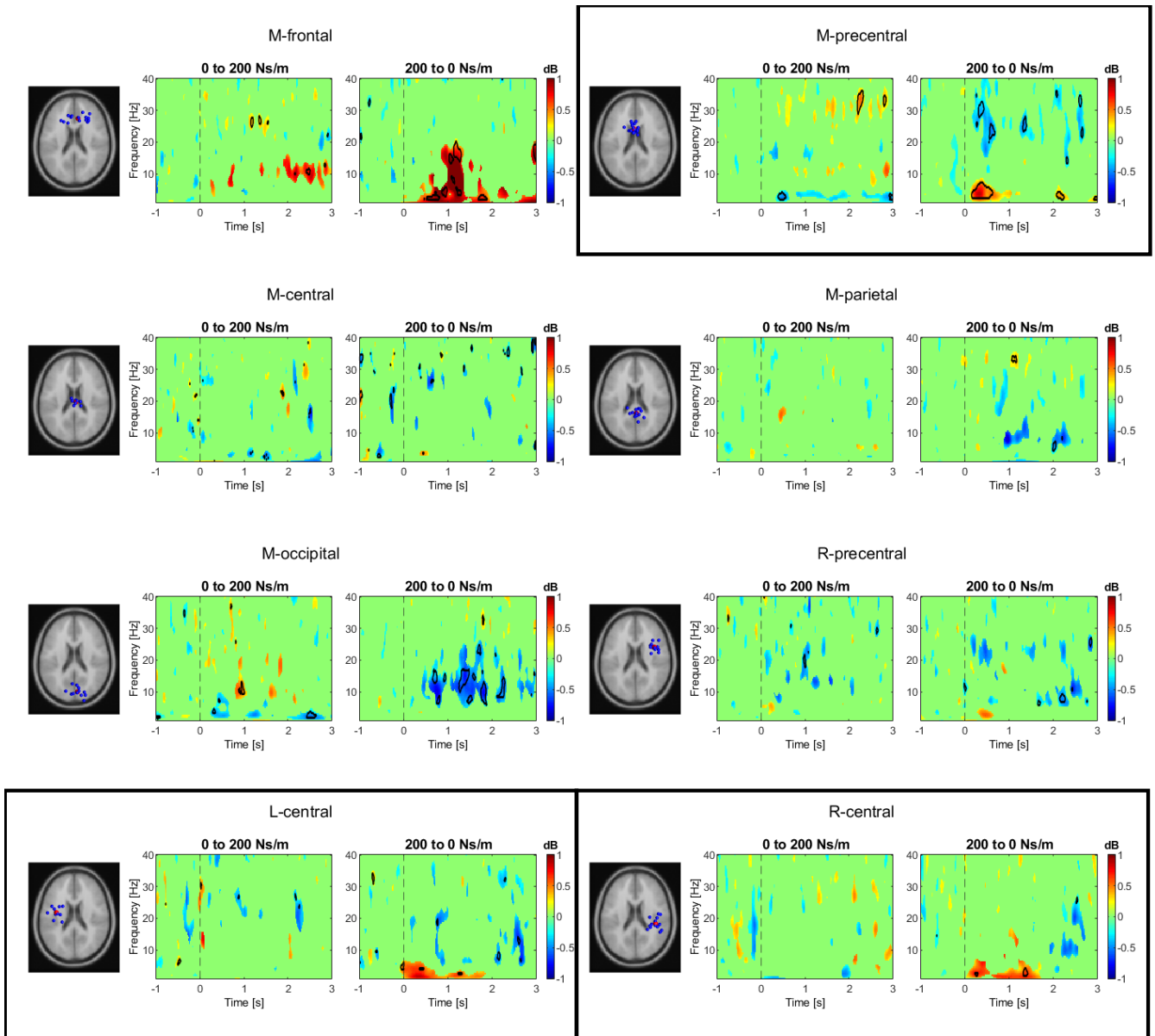


**Figure 9 | Event-related spectral perturbations time-frequency maps for the time-variant trials.** For each cluster the time-frequency maps show the mean power increase (red) or decrease (blue) in response to an instantaneous increase (left plot) or decrease (right plot) of the external damping value (set to 0 or 200 Ns/m). The dotted vertical line indicates the instantaneous damping transition (at time = 0 s). The maps are masked for significance ( $p < 0.05$ ) colouring the non-significant ERSP values green. The black contour lines indicate the significant modulations after correction for false discovery rate (FDR). The graphic on the left shows the dipole locations of the individual components within a cluster (blue spheres) and the centroid location (red sphere). The clusters showing modulations immediately after an external damping change are highlighted with black boxes.

the response to an external damping increase (0 to 200 Ns/m) and damping decrease (200 to 0 Ns/m) separately. The maps are masked for significance ( $p < 0.05$ ) displaying non-significant ERSP values in green. The contours indicate the modulations that remain significant after correction for false discovery rate (FDR). (Time-frequency maps without significance masking are incorporated in the Supplementary Figures) Both the results that remained significant after FDR, as well as the modulations that did not survive this stringent correction will be described below because of the exploratory nature of this study.

Most interesting results are considered to be the power modulations that follow immediately after a damping transition, since these results illustrate the first responding cortical areas related to a change in the environmental dynamics and subsequent expected adaptive motor control. Clusters presenting with fast modulations are highlighted with black boxes in figure 9.

A significant brief and strong enhancement of delta and theta rhythms was found in the cluster located in the SMA (M-precentral) immediately after external damping was removed, along with suppression of beta-II rhythms. Moreover, an opposite direction of

modulation was observed in the same cluster when external damping was added: a suppression of delta and theta rhythms and enhanced beta-I/beta-II rhythms. These modulation patterns appear to sustain after the damping transition.

In the lateralized clusters located centrally (above the sensorimotor cortex: L-central and R-central), enhanced delta and theta rhythms were observed directly following an external damping decrease. However, a significant modulation of brain rhythms when external damping was added was absent in these clusters. The fast modulations appeared to be strong but were not considered significant after FDR correction.

Additionally, some disperse modulations in response to an event appeared within one second in the cluster located above the right premotor cortex (R-precentral): brief enhancement of delta rhythms and suppression of beta-II rhythms following both external damping addition and removal. However, this trend is not very clear and did not survive the FDR correction. Similarly, no clear trends were found in the cluster located centrally on the midline (M-central).

In the cluster located in the posterior parietal cortex (PPC) (M-parietal), a period of strong suppression of alpha rhythms was apparent approximately one second after removal of the external damping. Similarly, sustained suppression of alpha and beta-I rhythms appeared in the cluster located in the occipital cortex (M-occipital), associated with the visual cortex, when damping was decreased. A shorter and less strong enhancement of alpha rhythms was seen in the same cluster when external damping was added.

Furthermore, broadband enhancement was found in the cluster located in the prefrontal cortex (M-frontal) associated with the anterior cingulate cortex (ACC). A strong brief enhancement of delta, theta, alpha and beta-I waves appeared around one second after external damping removal. Enhancement of alpha rhythms was observed at a later time point relative to event onset when external damping was added.

Overall, modulations in power following a damping transition were found primarily in the condition of external damping removal. In few clusters (M-precentral and M-occipital), power modulations appeared to be of opposite sign between the two conditions. The most promising results, which survived the correction for multiple testing, appeared in the cluster located above the SMA immediately following external damping removal. Additionally, modulations found in the cluster located in the ACC and visual cortex also remained significant after FDR correction.

## Discussion

This study was aimed at identifying cortical areas that contribute to the online regulation of joint stiffness by analysing the cortical dynamics in response to a changing environment during a posture control task. An increase in joint stiffness in the postural task having a constant high external damping ( $b_e=200$  Ns/m) as

compared to the task without external damping ( $b_e=0$  Ns/m) was accompanied by increased theta and beta rhythms in the left sensorimotor cortex and decreased delta rhythms in the SMA. Therefore, we speculate that these areas are important in the regulation and maintenance of joint stiffness during posture stabilization of the upper limb. Secondly, unexpected changes in the environmental viscous loads elicited immediate cortical modulations in the sensorimotor cortex as well as in the SMA and later on in the prefrontal and visual cortex implying a role for these cortical regions in the detection of an unexpected event and subsequent adaptation of the motor control strategy. Moreover, we found that modulations in cortical activity were primarily elicited by external damping removal and were less pronounced when external damping was added implicating differential control strategies might be used to adjust joint stiffness dependent on the effects of unexpected changes in terms of stability.

### Differential levels of control dependent on stability margins

Our findings demonstrating an increase in joint stiffness with added external damping are in line with previous studies using a similar experimental set-up. (Schouten et al., 2008; Van Der Helm et al., 2002) Using a neuromusculoskeletal model to estimate the intrinsic and reflexive contribution to the mechanical admittance separately, Schouten et al. (2008) found that this increase in joint stiffness is caused by increased reflexive feedback gains. Whereas high reflexive feedback gains are successful in decreasing mechanical admittance for the low frequencies (below the eigenfrequency of the shoulder  $\sim 2.5$  Hz), they also tend to decrease stability margins around the eigenfrequency due to neural time delays associated with reflexive feedback pathways. The addition of external damping, however, suppresses oscillations around the eigenfrequency and therefore the combined arm-environment system remains well-damped and stable. Unexpected removal of this external damping puts the system at risk for instability worsening performance, whereas the unexpected addition of external damping adds to the stability margins and does not worsen the performance.

We found that an instantaneous external damping removal (from 200 to 0 Ns/m) elicited responses in the SMA, sensorimotor cortex, prefrontal and visual cortex, whereas the addition of viscous loads (from 0 to 200 Ns/m) elicited limited modulations only in the SMA and visual cortex. (see Figure 9) These differential cortical responses between an environmental change leading to decreased or increased stability margins, respectively, suggest that the CNS might use different control strategies dependent on the stability margins.

The lack of regulatory activity in the cortex when external damping is added as seen in this study suggests that the modulation of joint stiffness might either occur at a later time point relative to the damping transition or that regulation might occur on a different level when stability is not at risk. Whereas this study is aimed at identifying key players on the cortical level, studies on the

---

contribution of spinal circuits to motor control have revealed a high level of functional flexibility present in responses mediated on the spinal level. (Fink et al., 2014; Nielsen, 2016; Weiler et al., 2019) Due to a complex network of inhibitory connections between interneurons and motor neurons, which integrate signals both originating from supraspinal areas as well as from sensory afferents and local neuronal inputs, motor output can be controlled. (Fink et al., 2014; Rudomin & Schmidt, 1999) Therefore, we hypothesize that regulatory mechanisms on the spinal level might suffice to adapt motor control when stability is not at risk, whereas a transcortical pathway is involved when stability is compromised.

Alternatively, it could be that adaptation of joint stiffness within trials is only present when external damping is decreased and not when viscous loads are added. The current methods did not allow for estimation of the joint stiffness over time when damping was changed within a trial. However, since there is substantial research showing that feedback responses present with a high level of functional sophistication and are modulated as to achieve near-optimal motor control (for review, see (Pruszynski & Scott, 2012)), we expect adapted joint stiffness within trials even if stability is not compromised as to maximize performance. The use of time-varying techniques to estimate admittance throughout the trials would be useful as to exclude this possibility.

### **Cortical control in the maintenance of joint stiffness**

Enhanced theta and beta power occurred in the left sensorimotor cortex (S1/M1) when external damping was present. (see Figure 8) An increase in power in this area is typically associated with a less active state of the sensorimotor cortex, related to decreased sensory processing or descending motor commands. (Neuper & Pfurtscheller, 2001) To minimize the effect of sensory input on the cortical activity, we aimed to average out the continuous sensory activity in the brain through the use of uncorrelated disturbance signals exciting the sensory system in a different way each trial. Additionally, by scaling the disturbance forces separately for the high and low damping condition, we ensured similar muscle stretch lengths. Therefore, the increase in theta and beta rhythms with external damping present is most likely linked to decreased efferent motor commands related to feed-forward or feedback motor control. Both control mechanisms (feed-forward and feedback) are involved in the regulation of joint stiffness affecting the intrinsic and reflexive contribution, respectively. (Ludvig et al., 2007) The finding that the change in joint stiffness is primarily caused by a change in the reflexive contribution using similar experimental conditions (Schouten et al., 2008), suggests that feedback control is the primary mechanism responsible for the observed change in joint stiffness. Thus the observed decrease in power in the sensorimotor cortex with external damping present might represent decreased top-down input related to feedback control. Pre-synaptic inhibitory input arising from corticospinal neurons has been suggested as the primary mechanism to

modulate reflex gains. (Stein & Capaday, 1988) Our findings support the idea that the sensorimotor cortex is involved in regulating and maintaining joint stiffness possibly through descending inhibiting neural commands onto the spinal level therewith influencing reflex sensitivity. However, a direct causal relationship cannot be established from our results neither can we exclude the possibility that sensory processing was also represented in the cortical activity.

Furthermore, delta power in the SMA appeared to be significantly less with external damping present. Oscillations in the delta frequency band have been linked to processes of cortical inhibition and functional cortical deafferentiation (Harmony, 2013; John & Prichep, 2006), which might suggest a role for the SMA in modulating activity of other brain regions like the sensorimotor cortex as to aid in the selection of the appropriate control strategy.

### **Cortical involvement in the adaptation of joint stiffness**

A strong brief enhancement of delta and theta rhythms along with suppressed beta-II rhythms was elicited in the SMA by an external damping transition from 200 to 0 Ns/m. (see Figure 9) The immediate response found in the SMA implies a critical role for the SMA in the detection of a change in the environmental dynamics being one of the first responding cortical areas (together with the sensorimotor cortex). Additionally, broadband enhancement of delta, theta, alpha and beta rhythms was found in the prefrontal cortex. Similar patterns of enhancement in studies on postural balance control following a perturbation challenging stability have been reported (Mierau et al., 2017; Solis-Escalante et al., 2019). In a study focused at identifying neural contributors to wrist stabilization using functional MRI, the SMA and prefrontal cortex were also implicated to be important in the optimization of feedback control. (Suminski et al., 2007) Additionally, it has been argued that theta band activity in the prefrontal cortex represents the realization of the need for cognitive control and subsequent implementation of adaptive control. (Cavanagh & Frank, 2014) Therefore, these enhancement patterns might illustrate important processing in the fronto-central networks involved with the detection of unexpected events challenging stability and subsequent adaptations of motor control.

Increased delta and theta rhythms appeared both in the left and right sensorimotor cortex following damping removal, which were noteworthy trends but did not survive the correction for false discovery rate. Nonetheless, they imply a role for the sensorimotor cortex in the modulation of joint stiffness upon removal of external damping possibly directed by the SMA. Especially the observation that the unexpected switch to the low damping environment resulted in enhanced theta power rhythms, whereas decreased theta band activity was found during the tasks having constant low damping as compared to the high-damping environment suggest that these modulations represent a different ongoing process. The cortical activity elicited by the damping decrease is therefore likely related to processes involved with the adaptation of joint stiffness.

The importance of the sensorimotor cortex in the adaptation of reflex gains induced by changes in the environmental dynamics has been shown before (Shemmell et al., 2009) and is underlined by our findings.

Lastly, suppression of alpha rhythms was apparent in the visual cortex as well as in the PPC following a decrease in external damping. These modulations are most likely to be linked to the processing of visual sensory input. During the measurements it was observed that the unexpected removal of the external damping resulted in a large shift in the position, which likely contributed to the found power modulations in the visual cortex.

## Limitations

The experimental methods used did not allow for the separation of the two distinct components of the mechanical admittance: the intrinsic and reflexive contributions. Therefore, we are not able to directly link cortical activity to modulated reflexive pathways, even though modulation of reflex gains has been implicated as the primary mechanism in joint stiffness adaptation. (Schouten et al., 2008) Separating the reflexive and intrinsic components in time-variant conditions requires the use of alternative methods and warrants further research.

Whereas EEG has a high temporal resolution, no implications for the timing of certain processing activities were made based on the time-frequency maps. In calculating event-related spectral perturbations (ERSPs), a trade-off exists between frequential and temporal resolution. In the present study, a time window of approximately 1.5 seconds was used for the lowest frequencies and therefore care was taken when drawing conclusions concerning the timing of found modulations. A higher temporal precision could be achieved by using the original data instead of the downsampled data for the calculation of ERSPs.

Another limitation of this study is that we did not incorporate the contribution of subcortical structures, like the cerebellum and basal ganglia, whereas they have been linked to the processing of sensory feedback before. (Scott, 2012) Therefore, future studies on brain mechanisms in adaptive motor control might include the contribution of subcortical control loops as well by using alternative source modelling methods using EEG recordings (Attal et al., 2012) or using alternative methods for measuring brain activity, like functional MRI.

## Concluding remarks

The neural mechanisms underlying the processing of feedback to adjust control strategies like adaptation of the joint stiffness over time have not received much attention. The present study examined the spectral perturbations in the cortex elicited by a change in the environmental mechanics during a postural precision task using the upper limb. The sensorimotor cortex as well as the SMA and prefrontal cortex may be key players in the adaptation process of joint stiffness as illustrated by the found power modulations following an unexpected removal of external damping. Moreover, the control processes to adapt joint stiffness

might occur on a different level (cortical vs spinal) dependent on the risk to instability. This study provides a first clue about possible cortical contributors in the process of joint stiffness adaptation in the upper limb. Understanding the neural mechanisms involved with joint stiffness adaptation aids in the diagnosis of patients with neurological damage and contributes to improved personalized treatment plans. Future studies should be directed at establishing causal relationships between cortical processing activities and the adaptation of control strategies. One possible way to achieve this is through stimulation or inhibition of specific cortical regions using techniques like transcranial direct current stimulation (tDCS) or magnetic stimulation (TMS).

## Acknowledgements

Performing EEG research has been a novel experience for me and I certainly enjoyed most parts of it. I have learned it is a very time-consuming branch of research and requires a certain skill set, among which dedication and patience. Luckily, I did not have to figure out all of it on my own. I have had a lot of help from my supervisor Mark van de Ruit and I would like to thank him for helping me with the experimental set-up, the measurements, thinking along in finding the best approach for the data analysis and for commenting on my thesis. I would also like to thank Alfred Schouten for giving useful comments on this article. To acquire sufficient EEG data, participants had to perform many repetitions of the same task, which required around 3-4 hours. Therefore, many thanks to the volunteers that participated. Lastly, the support of friends and family were of great value and indispensable, thanks to you all!

## References

- Abbruzzese, G., Berardelli, A., Rothwell, J. C., Day, B. L., & Marsden, C. D. (1985). Cerebral potentials and electromyographic responses evoked by stretch of wrist muscles in man. *Experimental Brain Research*, *58*(3), 544–551. <https://doi.org/10.1007/BF00235870>
- Attal, Y., Maess, B., Friederici, A., & David, O. (2012). Head models and dynamic causal modeling of subcortical activity using magnetoencephalographic/electroencephalographic data. *Reviews in the Neurosciences*, *23*(1), 85–95. <https://doi.org/10.1515/rns.2011.056>
- Bell, A. J., & Sejnowski, T. J. (1995). An information-maximization approach to blind separation and blind deconvolution. *Neural Computation*, *7*(6), 1129–1159. <https://doi.org/10.1162/neco.1995.7.6.1129>
- Cavanagh, J. F., & Frank, M. J. (2014). Frontal theta as a mechanism for cognitive control. *Trends in Cognitive Sciences*, *18*(8), 414–421. <https://doi.org/10.1016/j.tics.2014.04.012>
- Cheney, P. D., & Fetz, E. E. (1984). Corticomotoneuronal cells contribute to long-latency stretch reflexes in the rhesus monkey. *The Journal of Physiology*, *349*(1), 249–272. <https://doi.org/10.1113/jphysiol.1984.sp015155>
- Chikara, R. K., & Ko, L. W. (2019). Modulation of the visual to auditory human inhibitory brain network: An EEG dipole source localization study. *Brain Sciences*, *9*(9), 216. <https://doi.org/10.3390/brainsci9090216>
- De Gooijer-Van De Groep, K. L., De Vlugt, E., De Groot, J. H., Van Der Heijden-Maessen, H. C., Wielheesen, D. H., Van Wijlen-Hempel, R. S., Arendzen, J. H., & Meskers, C. G. (2013). Differentiation between non-neural and neural

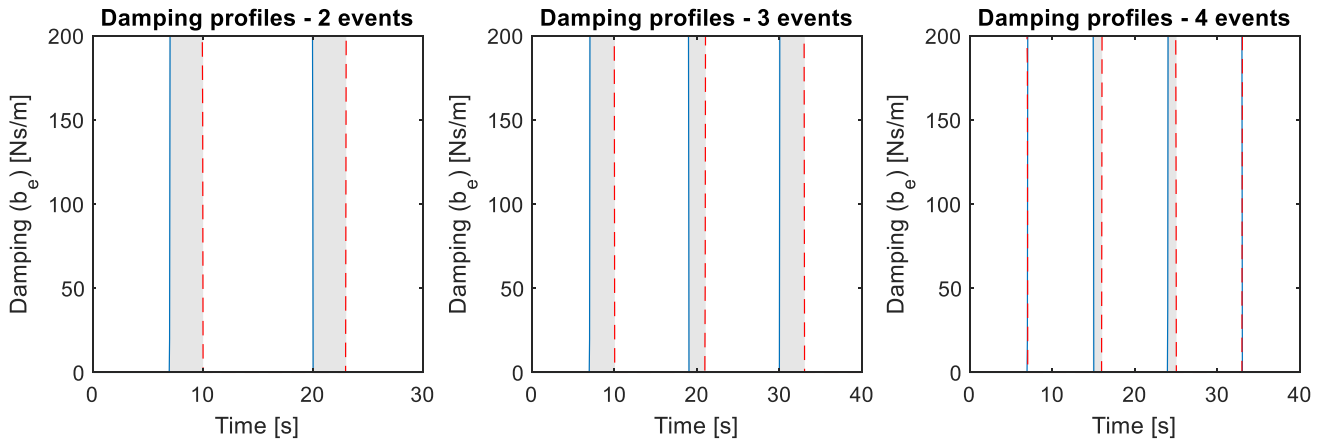
- contributors to ankle joint stiffness in cerebral palsy. *Journal of NeuroEngineering and Rehabilitation*, *10*(1), 1–8. <https://doi.org/10.1186/1743-0003-10-81>
- De Vlugt, E., Schouten, A. C., & Van Der Helm, F. C. T. (2002). Adaptation of reflexive feedback during arm posture to different environments. *Biological Cybernetics*, *87*(1), 10–26. <https://doi.org/10.1007/s00422-002-0311-8>
- Delorme, A., & Makeig, S. (2004). EEGLAB: An open source toolbox for analysis of single-trial EEG dynamics including independent component analysis. *Journal of Neuroscience Methods*, *134*(1), 9–21. <https://doi.org/10.1016/j.jneumeth.2003.10.009>
- Delorme, A., Palmer, J., Onton, J., Oostenveld, R., & Makeig, S. (2012). Independent EEG sources are dipolar. *PLoS ONE*, *7*(2). <https://doi.org/10.1371/journal.pone.0030135>
- Engel, A. K., & Fries, P. (2010). Beta-band oscillations—signalling the status quo? *Current Opinion in Neurobiology*, *20*(2), 156–165. <https://doi.org/10.1016/j.conb.2010.02.015>
- Evarts, E. V., & Tanji, J. (1976). Reflex and intended responses in motor cortex pyramidal tract neurons of monkey. *Journal of Neurophysiology*, *39*(5), 1069–1080. <https://doi.org/10.1152/jn.1976.39.5.1069>
- Fink, A. J. P., Croce, K. R., Huang, Z. J., Abbott, L. F., Jessell, T. M., & Azim, E. (2014). Presynaptic inhibition of spinal sensory feedback ensures smooth movement. *Nature*, *508*(7498), 43–48. <https://doi.org/10.1038/nature13276>
- Fromm, C., & Evarts, E. V. (1977). Relation of motor cortex neurons to precisely controlled and ballistic movements. *Neuroscience Letters*, *5*(5), 259–265. [https://doi.org/10.1016/0304-3940\(77\)90076-3](https://doi.org/10.1016/0304-3940(77)90076-3)
- Harmony, T. (2013). The functional significance of delta oscillations in cognitive processing. *Frontiers in Integrative Neuroscience*, *7*, 83. <https://doi.org/10.3389/fnint.2013.00083>
- John, E. R., & Pritchep, L. S. (2006). The relevance of QEEG to the evaluation of behavioral disorders and pharmacological interventions. *Clinical EEG and Neuroscience*, *37*(2), 135–143. <https://doi.org/10.1177/155005940603700210>
- Jung, T. P., Makeig, S., Mckeown, M. J., Bell, A. J., Lee, T. E. W., & Sejnowski, T. J. (2001). Imaging brain dynamics using component analysis. *Proceedings of the IEEE*, *89*(7), 1107–1122. <https://doi.org/10.1109/5.939827>
- Kearney, R. E., & Hunter, I. W. (1990). System identification of human joint dynamics. *Critical Reviews in Biomedical Engineering*, *18*(1), 55–87.
- Kimura, T., Haggard, P., & Gomi, H. (2006). Transcranial magnetic stimulation over sensorimotor cortex disrupts anticipatory reflex gain modulation for skilled action. *Journal of Neuroscience*, *26*(36), 9272–9281. <https://doi.org/10.1523/JNEUROSCI.3886-05.2006>
- Klimesch, W. (1999). EEG alpha and theta oscillations reflect cognitive and memory performance: A review and analysis. *Brain Research Reviews*, *29*(2–3), 169–195. [https://doi.org/10.1016/S0165-0173\(98\)00056-3](https://doi.org/10.1016/S0165-0173(98)00056-3)
- Krutky, M. A., Ravichandran, V. J., Trumbower, R. D., & Perreault, E. J. (2010). Interactions between limb and environmental mechanics influence stretch reflex sensitivity in the human arm. *Journal of Neurophysiology*, *103*(1), 429–440. <https://doi.org/10.1152/jn.00679.2009>
- Lancaster, J. L., Woldorff, M. G., Parsons, L. M., Liotti, M., Freitas, C. S., Rainey, L., Kochunov, P. V., Nickerson, D., Mikiten, S. A., & Fox, P. T. (2000). Automated Talairach Atlas labels for functional brain mapping. *Human Brain Mapping*, *10*(3), 120–131. [https://doi.org/10.1002/1097-0193\(200007\)10:3<120::AID-HBM30>3.0.CO;2-8](https://doi.org/10.1002/1097-0193(200007)10:3<120::AID-HBM30>3.0.CO;2-8)
- Lee, R. G., & Tatton, W. G. (1975). Motor Responses to Sudden Limb Displacements in Primates with Specific CNS Lesions and in Human Patients with Motor System Disorders. *Canadian Journal of Neurological Sciences*, *2*(3), 285–293. <https://doi.org/10.1017/S0317167100020382>
- Lee, T. W., Girolami, M., & Sejnowski, T. J. (1999). Independent component analysis using an extended infomax algorithm for mixed subgaussian and supergaussian sources. *Neural Computation*, *11*(2), 417–441. <https://doi.org/10.1162/089976699300016719>
- Ludvig, D., Cathers, I., & Kearney, R. E. (2007). Voluntary modulation of human stretch reflexes. *Experimental Brain Research*, *183*(2), 201–213. <https://doi.org/10.1007/s00221-007-1030-0>
- Ludvig, D., & Kearney, R. E. (2007). Real-time estimation of intrinsic and reflex stiffness. *IEEE Transactions on Biomedical Engineering*, *54*(10), 1875–1884. <https://doi.org/10.1109/TBME.2007.894737>
- MacKinnon, C. D., Verrier, M. C., & Tatton, W. G. (2000). Motor cortical potentials precede long-latency EMG activity evoked by imposed displacements of the human wrist. *Experimental Brain Research*, *131*(4), 477–490. <https://doi.org/10.1007/s002219900317>
- Makeig, S. (1993). Auditory event-related dynamics of the EEG spectrum and effects of exposure to tones. *Electroencephalography and Clinical Neurophysiology*, *86*(4), 283–293. [https://doi.org/10.1016/0013-4694\(93\)90110-H](https://doi.org/10.1016/0013-4694(93)90110-H)
- Makeig, S., Debener, S., Onton, J., & Delorme, A. (2004). Mining event-related brain dynamics. *Trends in Cognitive Sciences*, *8*(5), 204–210. <https://doi.org/10.1016/j.tics.2004.03.008>
- Makeig, S., Jung, T.-P., Bell, A. J., & Sejnowski, T. J. (1996). Independent component analysis of electroencephalographic data. *Advances in Neural Information Processing Systems*, *8*, 145–151.
- Mazzoni, P., Shabbott, B., & Cortés, J. C. (2012). Motor control abnormalities in Parkinson's disease. *Cold Spring Harbor Perspectives in Medicine*, *2*(6). <https://doi.org/10.1101/cshperspect.a009282>
- Meskers, C. G. M., Schouten, A. C., De Groot, J. H., De Vlugt, E., Van Hilten, B. J. J., Van Der Helm, F. C. T., & Arendzen, H. J. H. (2009). Muscle weakness and lack of reflex gain adaptation predominate during post-stroke posture control of the wrist. *Journal of NeuroEngineering and Rehabilitation*, *6*(1), 29. <https://doi.org/10.1186/1743-0003-6-29>
- Mierau, A., Pester, B., Hülsdünker, T., Schiecke, K., Strüder, H. K., & Witte, H. (2017). Cortical Correlates of Human Balance Control. *Brain Topography*, *30*(4), 434–446. <https://doi.org/10.1007/s10548-017-0567-x>
- Mizrahi, J. (2015). Mechanical impedance and its relations to motor control, limb dynamics, and motion biomechanics. *Journal of Medical and Biological Engineering*, *35*(1), 1–20. <https://doi.org/10.1007/s40846-015-0016-9>
- Neuper, C., & Pfurtscheller, G. (2001). Event-related dynamics of cortical rhythms: Frequency-specific features and functional correlates. *International Journal of Psychophysiology*, *43*(1), 41–58. [https://doi.org/10.1016/S0167-8760\(01\)00178-7](https://doi.org/10.1016/S0167-8760(01)00178-7)
- Nielsen, J. B. (2016). Human Spinal Motor Control. *Annual Review of Neuroscience*, *39*, 81–101. <https://doi.org/10.1146/annurev-neuro-070815-013913>
- Omrani, M., Murnaghan, C. D., Pruszynski, J. A., & Scott, S. H. (2016). Distributed task-specific processing of somatosensory feedback for voluntary motor control. *eLife*, *5*. <https://doi.org/10.7554/eLife.13141>
- Oostenveld, R., & Praamstra, P. (2001). The five percent electrode system for high-resolution EEG and ERP measurements. *Clinical Neurophysiology*, *112*(4), 713–719. [https://doi.org/10.1016/S1388-2457\(00\)00527-7](https://doi.org/10.1016/S1388-2457(00)00527-7)
- Perreault, E. J., Chen, K., Trumbower, R. D., & Lewis, G. (2008). Interactions with compliant loads alter stretch reflex gains but not intermuscular coordination. *Journal of Neurophysiology*, *99*(5), 2101–2113. <https://doi.org/10.1152/jn.01094.2007>
- Pion-Tonachini, L., Kreutz-Delgado, K., & Makeig, S. (2019). ICLabel: An automated electroencephalographic independent component classifier, dataset, and website. *NeuroImage*, *198*, 181–197. <https://doi.org/10.1016/j.neuroimage.2019.05.026>
- Pruszynski, J. A., & Scott, S. H. (2012). Optimal feedback control and the long-latency stretch response. *Experimental Brain Research*, *218*(3), 341–359. <https://doi.org/10.1007/s00221-012-3041-8>
- Rudomin, P., & Schmidt, R. F. (1999). Presynaptic inhibition in the vertebrate spinal cord revisited. *Experimental Brain Research*, *129*(1), 1–37. <https://doi.org/10.1007/s002210050933>
- Schouten, A. C., Vlugt, E. De, Hilten, J. J. B. Van, & Helm, F. C. T. Van Der. (2008). Quantifying proprioceptive reflexes during position control of the human arm. *IEEE Transactions on Biomedical Engineering*, *55*(1), 311–321.
- Scott, S. H. (2012). The computational and neural basis of voluntary motor control and planning. *Trends in Cognitive Sciences*, *16*(11), 541–549. <https://doi.org/10.1016/j.tics.2012.09.008>
- Scott, S. H. (2016). A Functional Taxonomy of Bottom-Up Sensory Feedback Processing for Motor Actions. *Trends in Neurosciences*, *39*(8), 512–526.

---

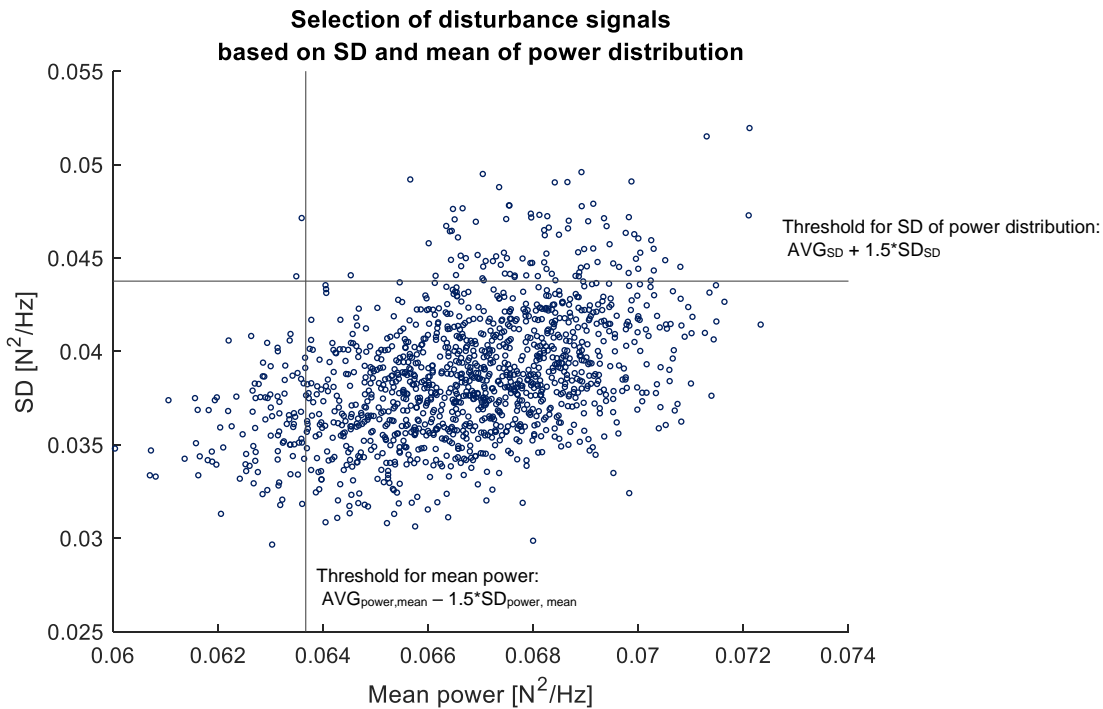
<https://doi.org/10.1016/j.tins.2016.06.001>

- Shemmell, J., Je, H. A., & Perreault, E. J. (2009). The differential role of motor cortex in stretch reflex modulation induced by changes in environmental mechanics and verbal instruction. *Journal of Neuroscience*, *29*(42), 13255–13263. <https://doi.org/10.1523/JNEUROSCI.0892-09.2009>
- Solis-Escalante, T., van der Crujisen, J., de Kam, D., van Kordelaar, J., Weerdesteyn, V., & Schouten, A. C. (2019). Cortical dynamics during preparation and execution of reactive balance responses with distinct postural demands. *NeuroImage*, *188*, 557–571. <https://doi.org/10.1016/j.neuroimage.2018.12.045>
- Spieser, L., Aubert, S., & Bonnard, M. (2013). Involvement of SMAp in the intention-related long latency stretch reflex modulation: A TMS study. *Neuroscience*, *246*, 329–341. <https://doi.org/10.1016/j.neuroscience.2013.05.005>
- Stein, R. B., & Capaday, C. (1988). The modulation of human reflexes during functional motor tasks. *Trends in Neurosciences*, *11*(7), 328–332. [https://doi.org/10.1016/0166-2236\(88\)90097-5](https://doi.org/10.1016/0166-2236(88)90097-5)
- Suminski, A. J., Rao, S. M., Mosier, K. M., & Scheidt, R. A. (2007). Neural and electromyographic correlates of wrist posture control. *Journal of Neurophysiology*, *97*(2), 1527–1545. <https://doi.org/10.1152/jn.01160.2006>
- Van Der Helm, F. C. T., Schouten, A. C., De Vlugt, E., & Brouwn, G. G. (2002). Identification of intrinsic and reflexive components of human arm dynamics during postural control. *Journal of Neuroscience Methods*, *119*(1), 1–14. [https://doi.org/10.1016/S0165-0270\(02\)00147-4](https://doi.org/10.1016/S0165-0270(02)00147-4)
- Weiler, J., Gribble, P. L., & Pruszynski, J. A. (2019). Spinal stretch reflexes support efficient hand control. *Nature Neuroscience*, *22*(4), 529–533. <https://doi.org/10.1038/s41593-019-0336-0>

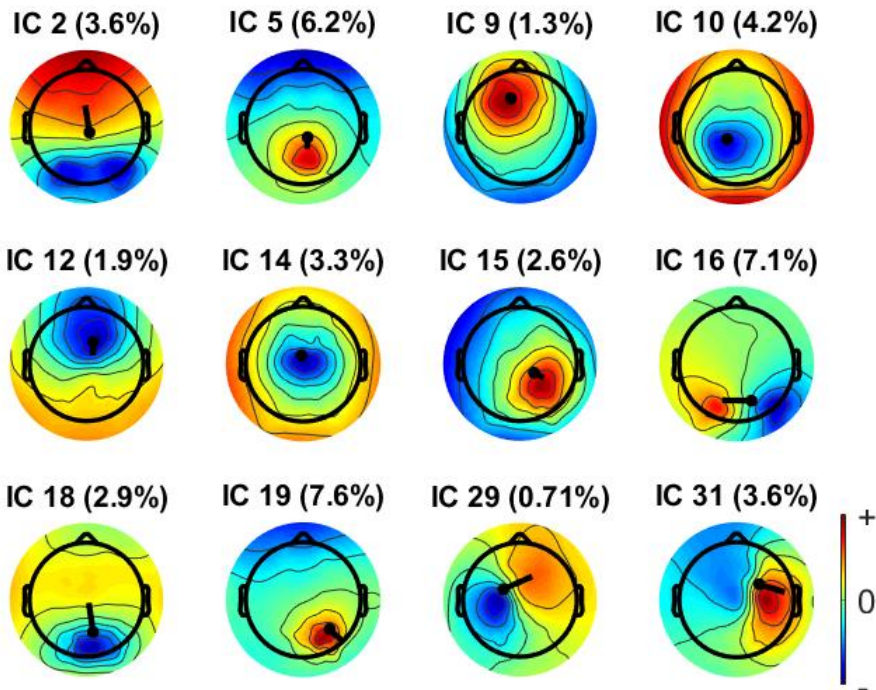
## Appendix A: Supplementary Figures and Tables



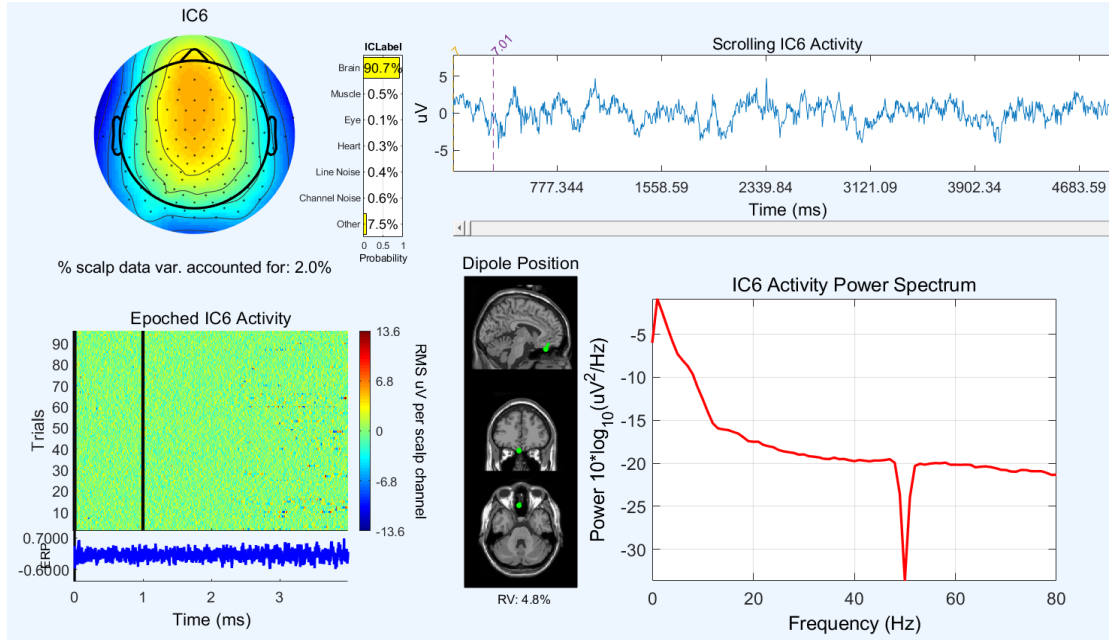
**Supplementary Figure 1 | Damping profiles for time-variant trials with two, three or four events.** The damping was changed rapidly (100 ms) from low to high damping or vice-versa at random times within pre-defined time intervals (shaded areas). Time intervals were chosen to ensure the damping remained constant for at least 8 seconds after a switch. Note that the trials with two events lasted 30 seconds, whereas trials with three or four events lasted 40 seconds. The time-invariant trials (damping profiles not shown) lasted 20 seconds.



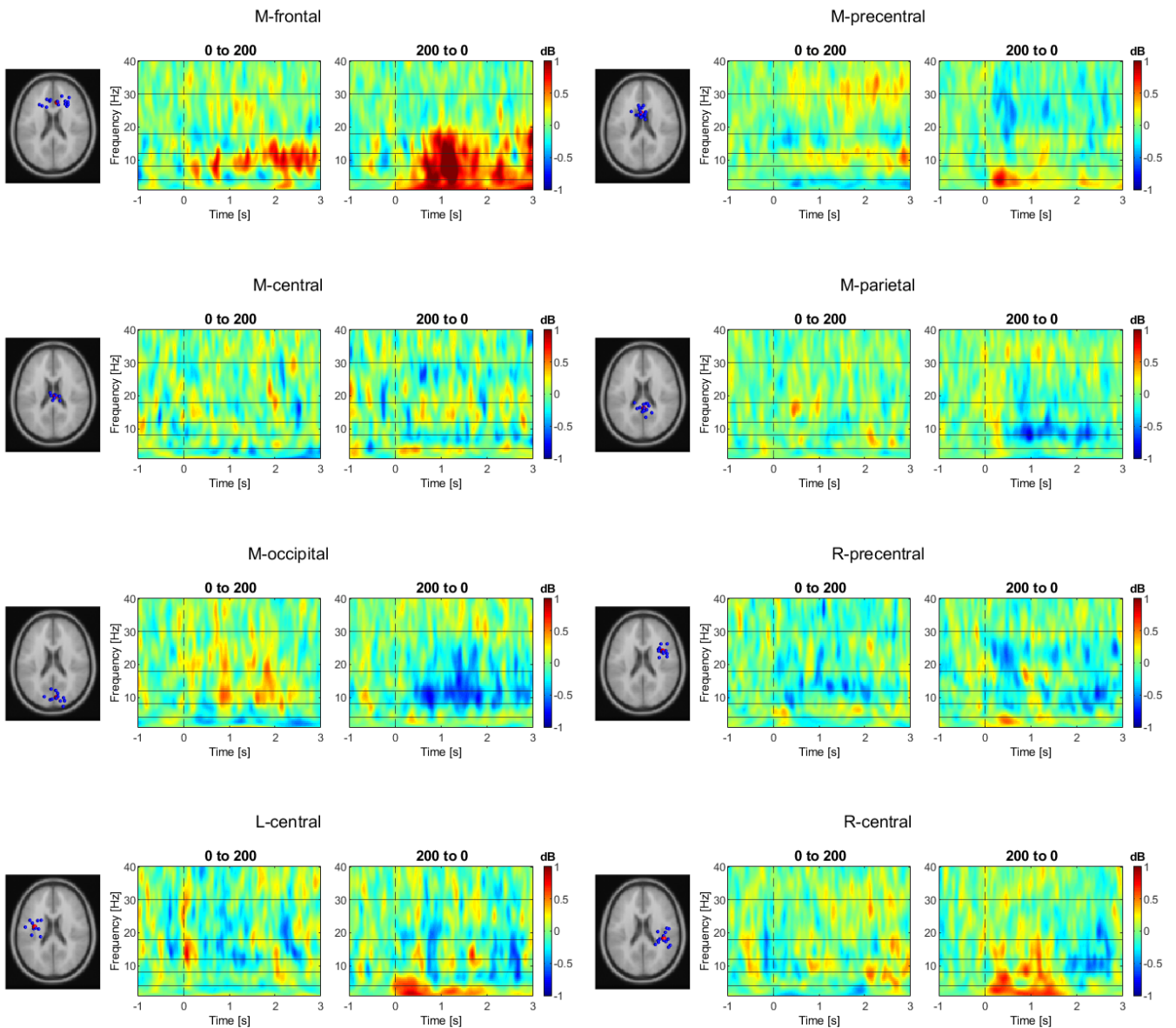
**Supplementary Figure 2 | Scatter plot of a set of disturbance signals showing the mean and SD of their power distribution.** Disturbance signals were selected based on their power distribution to obtain signals with a similar amount of power distributed equally over the frequencies up to 7 Hz (within the bandwidth). Each dot represents a disturbance signal having a mean power value (x-axis) and standard deviation (y-axis). The horizontal and vertical lines depict the thresholds for rejection which were set at a z-score  $>1.5$  for the SD and a z-score  $<-1.5$  for the average power.



**Supplementary Figure 3 | Example of selected ICs from one participant represented by their scalp map and equivalent current dipole.** Independent components were selected based on the classification label ('Brain'  $\geq 80\%$ ) and the residual variance after an equivalent current dipole fit ( $RV \leq 10\%$ ). The scalp maps shown here correspond to the ICs selected based on these two criteria. The fitted equivalent current dipoles are plotted for each IC and the percentage of unexplained variance is reported.



**Supplementary Figure 4 | Example of an IC rejected after visual inspection.** An additional visual inspection was performed identifying components with a physiologically irrelevant source location (e.g. behind the eyes) and components with an irregular activity between the trials presenting with peak amplitudes especially in the last 20 or 10 seconds. The latter were removed, because they most probably display brain activity occurring outside measurement time during the trials that only lasted 20 or 30 seconds. Visual inspection was performed using the summary of each IC as depicted here: scalp map + ICLabel classification (top left); Electrical activity throughout trials (bottom left) and the dipole location (bottom middle). Additionally, the component activity time course is displayed (top right) and the IC's power spectrum (bottom right).



**Supplementary Figure 5 | Event-related spectral perturbations time-frequency maps without significance masking.** For each cluster the time-frequency maps show the mean power increase (red) or decrease (blue) in response to an instantaneous increase (left plot) or decrease (right plot) of the external damping value (set to 0 or 200 Ns/m). The graphic on the left shows the dipole locations of the individual components within a cluster (blue spheres) and the centroid location (red sphere). The dotted vertical line indicates the damping transition (at time = 0 s). The vertical black lines mark the border between the general EEG frequency bands (delta: 1-4 Hz, theta: 4-8 Hz, alpha: 8-12 Hz, beta-I: 12-18 Hz, beta-II: 18-30 Hz).

---

**Supplementary Table 1 | Overview of included ICs per participant**

Participant number	Number of ICs after selection		
	Classification 'brain' > 80%	Residual variance < 10%	Visual inspection
1	18	11	10
2	20	14	13
3	33	29	<b>24</b>
4	21	16	12
5*	14	12	11
6	19	11	10
7	21	16	13
8	19	17	13
9*	33	28	<b>19</b>
10	27	24	<b>20</b>
11	12	8	8
12	10	8	6

\*Participants who did not follow the trend of increased joint stiffness in the task with constant high damping

**Supplementary Table 2 | Overview of number of included ICs per participant for each cluster**

Cluster label	Number of ICs included per participant											
	P1	P2	P3	P4	P5	P6	P7	P8	P9	P10	P11	P12
M-frontal	2	2	2	1	2		1	2	3			
M-precentral	1	3	2	3	1	1	2	2	1	1	1	2
M-central		1	2	1		1		1	1	1		
M-parietal		3	3	1	1		1		3	2	1	
M-occipital	1			1	2	2	2	1		2	1	
R-precentral		1	1	1	1	1			2	3	1	1
L-central	1		3	1	1	1	1	1	1	1		
R-central	1	1	3			1	2	2	2	3	1	

---

## Appendix B: Participant information letter

# PARTICIPANT INFORMATION SHEET

## Concerning a study investigating the dynamics of movement control using electroencephalography (EEG)

---

Date 20-07-2020, Version 2.0

Dear Participant,

You have been asked to participate in a study during which the dynamics of human motor control are explored, using a robotic manipulator and electroencephalography (EEG). This information sheet provides detailed information about the study.

### **Study background**

Humans use their reflexes to automatically react to unexpected external conditions, for example to protect themselves against harmful stimuli or disturbances. Reflexes also ensure coordinated use of different muscles, e.g. preventing two muscles to work against each other. It is likely our central nervous system (CNS) is able to unconsciously tune our reflexes to the conditions experienced. This reflex tuning can be disrupted when the CNS is damaged, for example following a stroke. Disrupted control of reflexes may result in movement disorders, like spasticity. Better understanding of how the CNS affects reflexes is important to allow for improved comprehension of movement disorders. In this study we specifically look at the speed with which humans are able to adapt their reflexes in response to changing environmental conditions and how the CNS controls these adaptations.

### **Study goal**

The goal of this study is to learn more about (1) which areas of the brain are active when adaptations to motor control are required and (2) how different data analysis techniques allow for accurate quantification of rapid adaptations in motor control.

### **What does participating involve?**

To study stretch reflexes in the shoulder, the shoulder muscles need to be rapidly stretched by moving the shoulder forward and backward. The study will be performed with a robotic manipulator that has been developed within Delft University of Technology. The device is hydraulically driven and connected to a personal computer which controls the position of a handle. You will be asked to firmly hold the handle with your right hand while the lower arm makes an approximate 90 degree angle with the upper arm. By holding the handle, the shoulder position will be automatically controlled. Throughout the study you will be instructed to try to resist the movement of the handle as to keep a constant position. Muscle activity will be measured by non-invasive electromyography (EMG), for which surface electrodes will be placed on four different muscles around the shoulder. Brain activity will be measured by electroencephalography (EEG), which is a non-invasive method to measure the electrical impulses travelling through the brain. These signals provide us insight in how the brain controls the tasks you are asked to perform. To measure EEG, you will be asked to wear a cap throughout the experiment in which measurement electrodes are integrated (see Figure 1). In order to have a good conductance between the skin and electrodes, each electrode will have some conducting gel. At the end of the experiment we will remove the gel as much as we can, but some remaining gel will have to be washed out at home.

The study takes place in the Laboratory for NeuroMuscular Control within the department of Biomechanical Engineering of the Delft University of Technology. The total experiment takes about 4 hours including set-up and removal of the measurement equipment. Regular breaks are provided and extra short pauses can be requested anytime throughout the experiment by the participant.

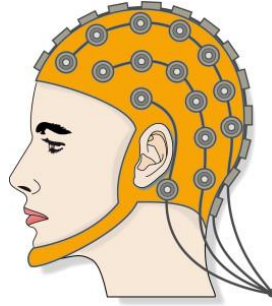


**Figure 1: Measuring electroencephalography (EEG)**

### **Participation preparations**

We ask participants to withhold from taking caffeinated drinks, like coffee, on the day of the experiment, since this might influence resting brain activity. Additionally, we would like to ask you to wash your hair the day before and not use any hair products on the day of the experiment so there are no remnants of hair products negatively impacting conductivity.

### **Risks**

Risks associated with the study are small. The movement of the shoulder is only in the order of a few centimetres and the movement of the handle is limited to prevent large movements. All hydraulics and moving or fragile parts are covered. Recording of EMG and EEG are routine research and clinical procedures which are performed daily without known harmful effects or significant risks

### **Participation is voluntary!**

Your participation in the study is voluntary. If you agree on participating in the study, you have the right to withdraw at any time (also during the study). There is no need to have a legitimate reason to do so. In case you agree to participate in the study you will be provided an informed consent form for you to sign.

### **Confidentiality**

We will treat your personal details and data confidentially. People not authorised to access your details will not have the opportunity to do so. When the results of the study get published, it is impossible to trace these back to you.

### **Summary**

Participating in this study is voluntary. Summarized, when you decide to participate:

- You are willing to participate in research during which EMG and EEG measurement will be performed while you perform simple movement control tasks;
- You adhere to the asked preparations on the before and the day of the experiment;
- You agree with the use of your data for purposes of the study;
- You understand we cannot provide individual study results.

For more information, feel free to contact one of the researchers mentioned below.

Thanks in advance for considering participation in our study!

Kirsten Nijmeijer (first point of contact)  
MSc. student Biomedical Engineering

Mark van de Ruit  
Postdoctoral researcher